A&A 596, A76 (2016)
DOI: 10.1051/0004-6361/201628531

Astronomy & Astrophysics

H_α-activity and ages for stars in the SARG survey[⋆,⋆⋆]

E. Sissa[1,2], R. Gratton[1], S. Desidera[1], A. F. Martinez Fiorenzano[3], A. Bonfanti[2], E. Carolo[1], D. Vassallo[1,2], R. U. Claudi[1], M. Endl[4], and R. Cosentino[3,5]

[1] INAF–Osservatorio Astronomico di Padova, Vicolo dell'Osservatorio 5, 35122 Padova, Italy
e-mail: elena.sissa@oapd.inaf.it
[2] Dipartimento di Fisica e Astronomia – Universita' di Padova, Vicolo dell'Osservatorio 3, 35122 Padova, Italy
[3] Fundación Galileo Galilei – INAF, Rambla José Ana Fernandez Pérez, 7, 38712 Breña Baja, TF, Spain
[4] McDonald Observatory, The University of Texas at Austin, Austin, TX 78712, USA
[5] INAF–Osservatorio Astrofisico di Catania, via S. Sofia 78, Catania, Italy

Received 16 March 2016 / Accepted 23 August 2016

ABSTRACT

Stellar activity influences radial velocity (RV) measurements and can also mimic the presence of orbiting planets. As part of the search for planets around the components of wide binaries performed with the SARG High Resolution Spectrograph at the TNG, it was discovered that HD 200466A shows strong variation in RV that is well correlated with the activity index based on H_α. We used SARG to study the H_α line variations in each component of the binaries and a few bright stars to test the capability of the H_α index of revealing the rotation period or activity cycle. We also analysed the relations between the average activity level and other physical properties of the stars. We finally tried to reveal signals in the RVs that are due to the activity. At least in some cases the variation in the observed RVs is due to the stellar activity. We confirm that H_α can be used as an activity indicator for solar-type stars and as an age indicator for stars younger than 1.5 Gyr.

Key words. binaries: visual – stars: activity – techniques: radial velocities – techniques: spectroscopic

1. Introduction

Studying the variation in the radial velocity (RV) induced by the chromospheric activity is important to distinguish it from the Keplerian motion of the star that may be caused by a planet (see e.g. Queloz et al. 2001; Dumusque et al. 2011; Robertson et al. 2014). On long timescales the active regions can modify measured RVs by introducing a signal related to the stellar activity cycle, while on short timescales the rotational period can become evident.

The most widely used activity indicators are based on the Ca II H&K lines (Isaacson & Fischer 2010; Lovis et al. 2011; Gomes da Silva et al. 2011), which have been shown to correlate with the radial velocity jitter. Other lines were investigated and it was found that the H_α line can be a good alternative (Robinson et al. 1990; Strassmeier et al. 1990; Santos et al. 2010; Gomes da Silva et al. 2011). However the correlation of H_α with Ca II H&K indices is high for the most active stars but decreases at a lower activity level, and sometimes becomes an anti-correlation (Gomes da Silva et al. 2011). Similar results were also found by Cincunegui et al. (2007), who added, using simultaneous observations of stars with spectral type later than F, that the correlation is lost when studying individual spectra of single stars and there is no dependence on activity. The correlation between the averaged fluxes for the Ca II and H_α lines can be clarified by considering the dependence of the two indexes on the stellar colour or the spectral type, while the absence of a general relation between the simultaneous Ca II and H_α index can be due to difference in the formation region of the two lines (Cincunegui et al. 2007; Gomes da Silva et al. 2014). Studying the solar spectrum as a prototype and extrapolating the results to other stars, Meunier & Delfosse (2009) discovered that plages and filaments in the chromosphere contribute differently to Ca II and H_α lines: while plages contribute to the emission of all these lines, the absorption due to filaments is remarkable only for H_α. Therefore the saturation of the plage filling factor seems to enhance the correlation between the two indexes in case of high stellar activity and low filament contribution. On the other hand, the anti-correlation between the emission in Ca II and H_α for low active stars seems to depend only on a strong filament contrast if the filaments are well correlated with plages (see also Gomes da Silva et al. 2014).

A search for planets around the components of wide binaries was performed using the Spettrografo Alta Risoluzione *Galileo* (SARG) at the Telescopio Nazionale *Galileo* (TNG) in the past years. Two planetary companions were detected around HD 132563B and HD 106515A (Desidera et al. 2011, 2012). Carolo et al. (2014) found strong variations in the RVs of HD 200466A that could not be explained by a stable planetary system, but which were well correlated to a H_α based activity indicator, showing that they are due to an ~1100-day activity cycle. Stimulated by this finding, we started a systematic analysis of H_α in the binaries of the SARG sample to identify activity-induced RV variations and distinguish them from planetary signatures.

⋆ Based on observations made with the Italian Telescopio Nazionale *Galileo* (TNG) operated on the island of La Palma by the Fundación Galileo Galilei of the INAF (Istituto Nazionale di Astrofisica) at the Spanish Observatorio del Roque de los Muchachos of the Instituto de Astrofísica de Canarias.

⋆⋆ A table of the individual H_α measurements is only available at the CDS via anonymous ftp to cdsarc.u-strasbg.fr (130.79.128.5) or via http://cdsarc.u-strasbg.fr/viz-bin/qcat?J/A+A/596/A76

We report here on the main results of the activity study made within this survey. We also include the measurements for additional stars observed by our group for other programs carried out with SARG.

2. Observation and data reduction

SARG is the High Resolution Spectrograph at TNG, now decommissioned, which worked for about 12 yr beginning in 2000 (Gratton et al. 2001). The SARG survey was the first planet research program entirely dedicated to binary systems and aimed to determine the frequency of giant planets up to a few AU separation from their star in nearly equal-mass visual binaries using high-precision radial velocities. The sample of the survey included 47 pairs of stars from the HIPPARCOS Multiple Star Catalog (Perryman et al. 1997), considering binaries in the magnitude range $7.0 < V < 10.0$, with magnitude differences between the components $\Delta V < 1.0$, projected separations larger than 2″ (to avoid strong contamination of the spectra), parallaxes larger than 10 mas, and errors smaller than 5 mas, with $B - V > 0.45$ mag and spectral types later than F7. For more details on the sample see Desidera et al. (2007). The stars are typically at distance <50 pc from the Sun.

Between September 2000 and April 2012 we collected up to 81 spectra per star with a typical exposure time of 900 s for a total amount of more than 6000 science images.

In this work we also include six bright stars that were observed with SARG looking to search for hot-Neptunes orbiting planets (Gratton et al. 2009). For these stars the integration time was set at 600 s except for 61Cyg B and 40 Eri, for which it was shorter to avoid saturation of the images because of their higher luminosity. τ Cet, 51 Peg and ρ CrB were used as RVs reference stars during the survey, and their signal-to-noise ratio (S/N) is typically greater then 270. In addition, HD 166435 was observed as benchmark active star (Martínez Fiorenzano et al. 2005). We decided to include this star in our sample as well.

Our data set therefore consists of two sub samples: the binary sample and the bright stars sample. The first is unbiased with respect to activity (except for HD 114723, which was excluded because of its high rotation), while the latter has a bias toward low-activity stars except for HD 166435. For all the observations we used the SARG Yellow Grism (spectral range 4600−7900 Å) and the 0.27 arcsec slit to obtain a resolution $R = 144\,000$ with a 2×1 pixel binning. The observed spectral range was covered by two chips. The blue chip included the spectral range used for the RV determination: the accuracy was given by a iodine cell superimposing a forest of absorption lines used as reference for the AUSTRAL code (Endl et al. 2000), as shown in Desidera et al. (2011). The red chip data are affected by fringing effects at wavelengths longer than ~7000 Å; these were not used in our analysis. The depth of the iodine lines decreases toward longer wavelengths, and the lines are negligible at the wavelength of H_α.

Data reduction was performed with standard IRAF[1] procedures.

3. Stellar parameters

For a proper interpretation of the H_α measurements that we derived in Sect. 4, some stellar parameters were considered. We describe here the adopted sources or procedures to measure them.

Differential radial velocities were derived in Carolo (2012) and have a typical uncertainty of about 4 m/s for stars in the binary survey and less then 2 m/s for the bright stars.

We considered measurements of $\log R'_{HK}$ from the literature, with preference for studies including multi-epoch measurements to take temporal variations of activity into account. Overall, we retrieved $\log R'_{HK}$ for 36 stars from Wright et al. (2004), Isaacson & Fischer (2010), Desidera et al. (2006b), Strassmeier et al. (2000) and Gray et al. (2003). Finally, for the components of HD 8009, HD 30101, HD 121298, and HD 128041, the value of $\log R'_{HK}$ was derived from HIRES spectra available in the Keck[2] archive following the procedure described in Carolo et al. (2014).

For stars without $\log R'_{HK}$ values in the literature we estimated the value from the ratio of X-ray to bolometric luminosity, using the calibration by Mamajek & Hillenbrand (2008). This latter quantity was derived following the procedure described in Carolo et al. (2014) and Carolo (2012) for the sources identified in the ROSAT All Sky Survey (Voges et al. 1999, 2000) within 30″ from our target stars. For the binaries composing most of our sample, the components are not spatially resolved by ROSAT. We then assumed equal X-ray luminosity for the components. For stars that are not detected in the ROSAT All Sky Survey, this procedure yields an upper limit on $\log R'_{HK}$. The values of $\log R'_{HK}$ or the upper limits, as other additional parameters we used, are listed in Table A.1.

The projected rotational velocity, $v \sin i$, was obtained from a calibration of the full width at half maximum (FWHM) of the cross-correlation function of SARG spectra. Details width be presented elsewhere. For the single stars we adopted the $v \sin i$ from literature sources such as Valenti & Fischer (2005).

The effective temperature T_{eff} of the primaries was derived from the $B - V$ colour using the calibration by Alonso et al. (1996) and assuming no reddening, while for the secondaries we relied on the high-precision temperature difference measured as part of the differential abundance analysis of 23 binary systems in Desidera et al. (2004, 2006a) and preliminary results by Vassallo (2014) for the others. For the single stars (standard stars and targets of the hot-Neptune program) we adopted the effective temperature from high-quality spectroscopic studies (e.g. Valenti & Fischer 2005).

4. H_α index

Since the Ca II H&K lines wavelengths are not included in the SARG yellow grism spectral range, we defined a new activity index based on the H_α line to study the activity of the stars in this sample. We built an IDL procedure optimized for the SARG spectra format: we measured the instrumental flux (not corrected for the blaze function) in a wavelength interval centred on the line core, F_H, and in two additional intervals symmetrically located with respect to the centre, F_{c1} and F_{c2}. H_α is defined as $H_\alpha = 2F_H/(F_{c1} + F_{c2})$, where F_{c1} = flux[6558.80−6559.80 Å], F_H = flux[6562.60−6563.05 Å], and F_{c2} = flux[6565.20−6566.20 Å]. Since the SARG spectrograph was not built to study in the H_α spectral range, this line appears twice but close to the edges of two orders (close to the blue edge of the order 93 and to the red edge of the order 94), according to the RV of the star. When we choose a wider window for F_{c1} and F_{c2} or increase the distance from F_H, the number of spectra in which the selected wavelength exits the detector therefore

[1] Tody (1993).

[2] https://koa.ipac.caltech.edu/cgi-bin/KOA/nph-KOAlogin

increases. Our choice is the best compromise. For the same reason we were unable to use the H_α index that was used by other authors (e.g. Kürster et al. 2003; Boisse et al. 2009; Santos et al. 2010; Gomes da Silva et al. 2014): for each order one of the two continuum reference windows used by these authors is outside of the region covered by the detector. Furthermore, we were unable to use a reference continuum to estimate the continuum flux because it is difficult to define the proper blaze function given the presence of the extended wings of the photospheric H_α absorption. To make our measurement more reliable, we used the weighted mean of two H_α values when fluxes for all these spectral bands could be measured in both orders.

4.1. Error estimation

We then analysed the possible sources of errors.

Internal noise

We estimated the errors on the fluxes assuming photon noise.

The error on H_α index was then derived by error propagation:

$$err_{H\alpha} = H_\alpha \sqrt{\left(\frac{1}{SN_H}\right)^2 + \frac{1/c_{1err}^2 + 1/c_{2err}^2}{(F_{c1} + F_{c2})^2}} \quad (1)$$

where $SN_i = \sqrt{\text{gain} \cdot F_i}$, $c_{1err} = SN_{c1}/F_{c1}$, $c_{2err} = SN_{c2}/F_{c2}$. We note that because of the lower value of the blaze echelle function, the H_α indexes coming from the order 94 have a lower weight on average. HD 128041, HD 143144, HD 9911, 61 CygB and GJ 580A have high absolute radial velocities (RV < -50 km s^{-1}) so that their spectra are remarkably blueshifted. Their H_α indexes have a higher uncertainty because the H_α line is shifted out from the order 93 spectra, therefore we were only able to use the SARG order 94, which yields poorer results.

Systematic error

We also considered that several other sources of noise can introduce errors on the H_α index: flat fielding, background subtraction, bad pixels, instrumental instability, fringing, etc. All these contributions, added to the possible intrinsic variations of activity, increase the standard deviation of the H_α values ($\sigma_{H\alpha}$). τ Cet was used as a test target for this purpose. It is very bright and its $\Delta H\alpha$ variation is lower than 0.005 dex (peak to valley) with low levels of variability in $\log R'_{HK}$ from the literature. We studied the variation of τ Cet night by night. We note that the standard deviation of H_α is about 10 times the intrinsic photonic error, therefore we decided to add a jitter to our measurement. Errors significantly larger than the photon noise error have been reported in other cases of 1 Å wide activity indices from echelle spectra, see for instance Wright et al. (2004). We found that this increase does not depend on the activity level of the star. It is instead described by a relation with the stellar magnitude as shown in Fig. 1: $\sigma_{jitter} = \sqrt{(0.0028)^2 + (5.27 \times 10^{0.4V-6})^2}$. Our adopted jitter is compatible with the single night variations of τ Ceti and we rescaled it for other stars according to their magnitude. The dependence on magnitude is that expected for error sources as background subtraction.

Finally the error applied to each measurement of H_α is the sum of the photonic error and the instrumental jitter as derived above. As the jitter is significantly larger then the photon noise, individual errors on H_α index of a given star are very similar.

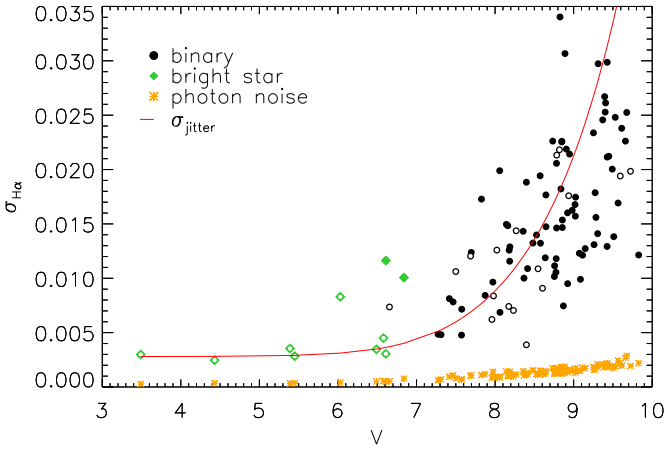

Fig. 1. Relation between V magnitude of the stars and the standard deviation $\sigma_{H\alpha}$ of the H_α index. Open symbols indicate quiet stars (see Sect. 4.3 for details), green diamonds are the bright stars sample. The continuous line represents the σ_{jitter} we adopted, while the orange asterisks indicate the mean photon noise value for each star.

Therefore the estimate of the jitter term has a very limited effect on the periodogram analysis presented in Sect. 6.

Contamination by telluric lines

In the spectral range of H_α we considered, there are several telluric lines mainly due to the water vapour. These lines can enter in our F_{c1}, F_{c2} and F_H intervals and influence the H_α index value. The strongest line is H_2O at 6564.206 Å. If this telluric line enters F_H, the H_α index will decrease of about 1.5%, giving an error by about 0.005 dex on a quiet star. This can occur when the geocentric velocity of the star is between 52 and 75 km s^{-1}. Therefore only a few of our spectra are involved, but none of those discussed below. The effect we have if this line enters F_{c2} is about 0.001 dex which is negligible. The H_2O line at 6560.555 Å can also enter the F_H interval with a comparable contribution if the geocentric radial velocities between −90 and −123 km s^{-1} are involved. These few spectra were rejected.

Contamination estimation

Even though during the observations of the binaries the slit was oriented perpendicularly to the separation of the components, some spectra are strongly contaminated by the companion star and were rejected. Furthermore we modelled the contamination for each consecutive observation of the companions assuming a Moffat-like shape for the point spread function (PSF) and taking into account the separation, the magnitude and the seeing. We obtain that the contribution of the contamination to the H_α is lower then 1% in the majority of the case and therefore is negligible. We found instead that for six systems the variation induced by the contamination is greater than the intrinsic variation (Fig. 2).

For example, HD 8071 is a very close binary system (ρ = 2.183″ according to HIPPARCOS) and the primary star is a spectroscopic binary with an amplitude of a few km s^{-1}. The effect of contamination on the RV is further modulated by the velocity of the primary at the observing epoch. This causes the RV to vary around the true value by up to a few hundreds m/s in a quite unpredictable way. For more details see Martínez Fiorenzano et al. (2005).

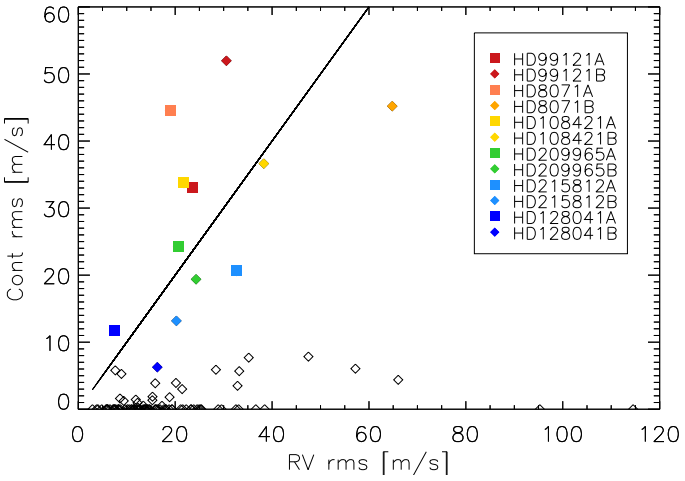

Fig. 2. Relation between the standard deviations of the RVs (after the correction for known Keplerian motions) and that induced by the contamination. Systems with a non-negligible contamination are highlighted.

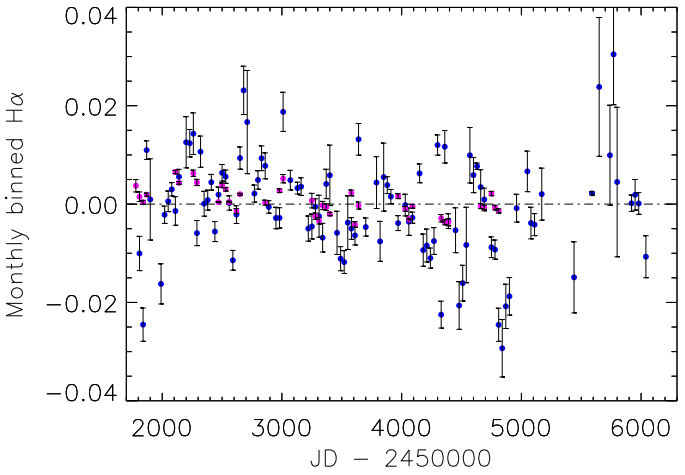

Fig. 3. Time evolution of the H_α values of all the spectra normalised to the median value for each star, monthly bins. The red points correspond to the τ Cet data series.

4.2. Stability of the instrument

The stability of the instrument during the survey was tested: for stars in the binary sample, we normalised the H_α value for each spectrum to the median value of its star. We then binned these values into the synodic monthly mean over different stars and compared them to the same results for the τ Cet data series (see Fig. 3). For τ Cet data we found that points are located around zero with $\sigma_{H\alpha} = 0.003$. For the stars in the binary sample, the last two years of the campaign were devoted to observing mainly a few stars with candidate companions and/or RV trends, therefore the H_α monthly means depend on the variability of the individual targets, as in the case of HD 200466 (Carolo et al. 2014). We also verified the presence of periodicity by applying the generalize Lomb-Scargle periodogram (GLSP) Zechmeister & Kürster (2009)[3] to the two sequences of the binned values: the whole sample sequence shows no significant peak and differs from the τ Ceti sequence, which shows a long-term trend (see Fig. 4).

[3] https://github.com/callumenator/idl/blob/master/Routines/Periodogram/generalised_lomb_scargle.pro

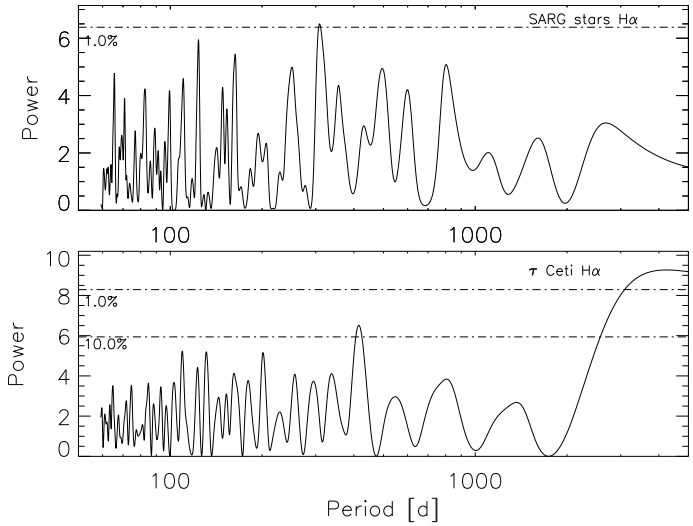

Fig. 4. GLSP of the synodic monthly binned H_α values of the SARG sample (*top*) compared to τ Cet (*bottom*).

4.3. Dependence on $T_{\rm eff}$ and $\Delta H\alpha$ definition

We divided our sample into two subgroups: as active stars we indicate stars with $\log R'_{\rm HK}$ greater than −4.80, the others are called quiet stars.

Since our H_α index is defined as the ratio between the flux in the line centre and the flux in the wings, we expect that different stars with the same activity level can have different $\langle H_\alpha \rangle$ values because of the different photospheric spectrum. Therefore we compared effective temperature and $\langle H_\alpha \rangle$ to determine the appropriate relation for quiet stars (Fig. 5).

Most of the quiet stars lie at $\langle H_\alpha \rangle \sim 0.22$ for $T_{\rm eff} > 5000$ K. At lower temperature, the $\langle H_\alpha \rangle$ index for quiet stars seems to increase. Active stars scatter mostly at higher $\langle H_\alpha \rangle$. We also made a comparison with the Sun: it has an effective temperature of 5780 K and its $\langle H_\alpha \rangle$ is 0.217, as measured in the solar flux atlas (Kurucz et al. 1984), in agreement with the lower envelope for quiet stars. We describe the distribution of the quiet stars in this lower envelope with a three-degree function and define as H_α-excess ($\Delta H\alpha$) the point distance from this line: $\Delta H\alpha$ is the difference in H_α index of a star with respect to a quiet star that has the same effective temperature. Therefore we decided to use $\Delta H\alpha$ as the activity index; it is more robust than H_α because it allows us to compare the activity of stars with different temperatures.

5. Sample analysis

5.1. Correlation with $\log R'_{\rm HK}$ and rotation

$\Delta H\alpha$ correlates quite well with $\log R'_{\rm HK}$ (reduced $\chi^2 = 2.26$, Fig. 6). Active stars are more scattered but typically show excess in the H_α index ($\Delta H\alpha > 0$). All the stars for which $\log R'_{\rm HK}$ has been derived from the X-ray luminosity are in the active portion of the diagram. This is due to the flux limit of the ROSAT All Sky Survey, which is only sensitive to the active stars at the typical distance of our program stars. The stars for which only upper limits are derived populate the lower envelope of the distribution in most cases: this is consistent with a low activity level.

This new index appears to show that stars are distributed in two groups, which suggests the presence of the Vaughan-Preston gap at $\Delta H\alpha = 0.02$ (Vaughan & Preston 1980). The results of Pace et al. (2009) also show the presence of a gap

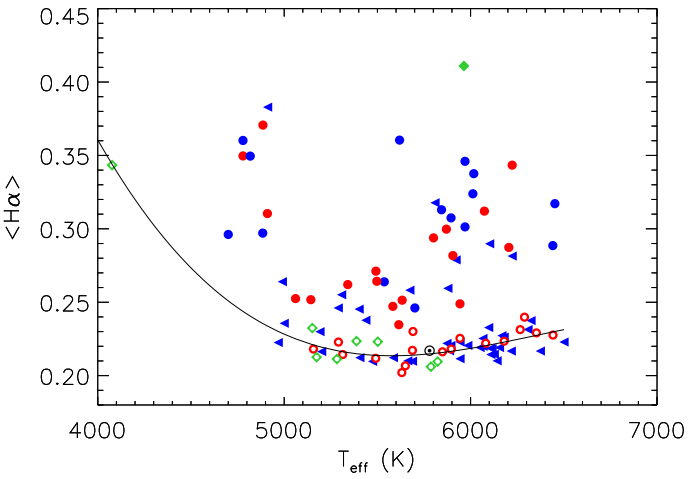

Fig. 5. Relation between the temperature and the median value of H_α for each star. Colours are given according to $\log R_{HK}$ value sources: values from the literature are plotted in red, while for the blue dots the values are derived from X-ray luminosity. The blue triangles indicate that the $\log R'_{HK}$ value for a star is only an upper limit. Green diamonds indicate the bright stars sample. Open symbols correspond to quiet stars. The line only shows the fit of the binaries to have a sample unbiased by activity. The line shows the best fit for the quiet stars. The position of the Sun is also shown with ⊙.

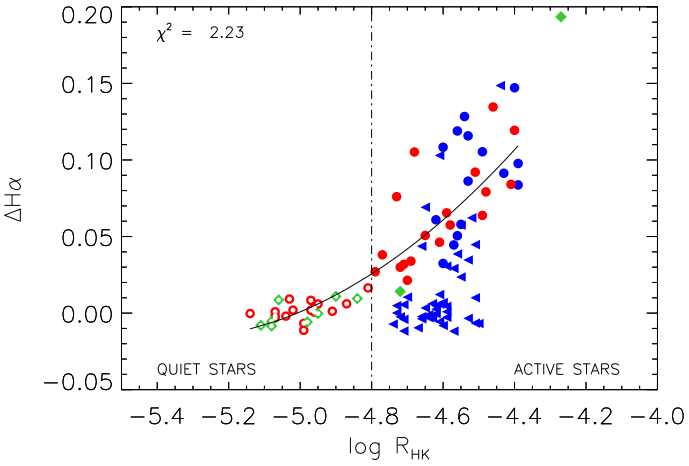

Fig. 6. Relation between the $\log R'_{HK}$ and $\Delta H\alpha$. Colours are the same as Fig. 5. Bright stars and stars with upper limits for $\log R'_{HK}$ were not considered to have a sample unbiased by activity.

between $\log R_{HK} = -4.7$ and -5.0. This corresponds to the interval $\Delta H_\alpha \sim [0.01, 0.04]$.

We also found a weak relation between $\Delta H\alpha$ and its standard deviation: the intrinsic variation of the H_α index and internal errors contribute to the increase in scatter in the H_α index measurement for each star, but since the scatter is dominated by intrinsic errors for fainter stars, only the deviation seen in brighter stars is dominated by the intrinsic variability.

We also checked the well-known relation between rotation and activity (e.g. Noyes et al. 1984; Baliunas & Vaughan 1985; Santos et al. 2000). We found, as expected, that a moderate rotation is enough to cause a high activity for cold stars and in this case the $v \sin i$ value increases with activity, while the hottest stars only have high activity values if $v \sin i$ is high: this behaviour can be related to the decrease in thickness of the convective envelope as the stars become hotter (Charbonneau & Steiner 2012).

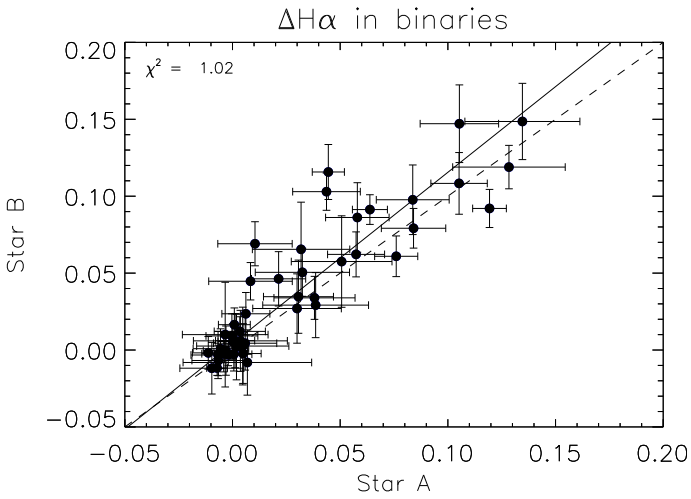

Fig. 7. Relation between the $\Delta H\alpha$ of the two companion stars. The solid line corresponds to the best fit, the dashed line corresponds to the equivalence.

5.2. Binary components

We can compare the $\Delta H\alpha$ index for the two components in each binary system: we find a very good relation between the two stars indexes, that is $\Delta H\alpha_B = (1.11 \pm 0.08)\Delta H\alpha_A + 0.004 \pm 0.004$, as shown in Fig. 7. The value of the reduced χ^2 suggests that the scatter is dominated by the measurement error. We tested that the long-scale activity cycles (like the solar cycle) induce a variation in H_α that is weaker than our adopted measurement error. HD 108421, HD 132844 and HD 105421 lie above the relation, but we did not note any evidence of errors in our analysis for these stars, so that the discrepancy seems to be real and the two stars of these systems could be in different activity phases. For HD 126246, which lies below the relation, the difference in the H_α activity level between the two components qualitatively agrees with the $\log R'_{HK}$ and $v \sin i$ difference found by Desidera et al. (2006a), supporting an intrinsic rotation and activity difference between the two components.

5.3. Age-activity relation

Prompted by this result, we tested whether our $\Delta H\alpha$ could be an age indicator for these stars (e.g. Skumanich 1972; Baliunas & Vaughan 1985; Soderblom et al. 1993; Mamajek & Hillenbrand 2008; Pace 2013; Zhao et al. 2011). We computed the ages of the binary systems with the isochrone fitting algorithm developed by Bonfanti et al. (2015). The implementations details can be found in Bonfanti et al. (2015, 2016). Here we recall that it enables recovering the isochronal age of a field star when at least its [Fe/H], T_{eff} and $\log g$ are available. In our case we also considered $\log R'_{HK}$ as input parameter, which allowed us to disregard unlikely very young isochrones, so that we could better constrain the stellar age. Since the evolution of low-mass stars is extremely slow, this method works well for stars with $T_{eff} > 5500$ K; for cooler (less massive) stars, uncertainties in the exact location of a star on the Hertzspurng-Russel (HR) diagram leads to an error so large that practically all ages from 0 up to the age of the Universe are possible. We therefore did not consider such stars in our test.

From the differential abundance analysis, T_{eff} and $\log g$ have typical uncertainties of ~50 K and ~0.15 dex, respectively, while the differences $\Delta T_{eff} = T_{effA} - T_{effB}$ and $\Delta \log g = \log g_A - \log g_B$

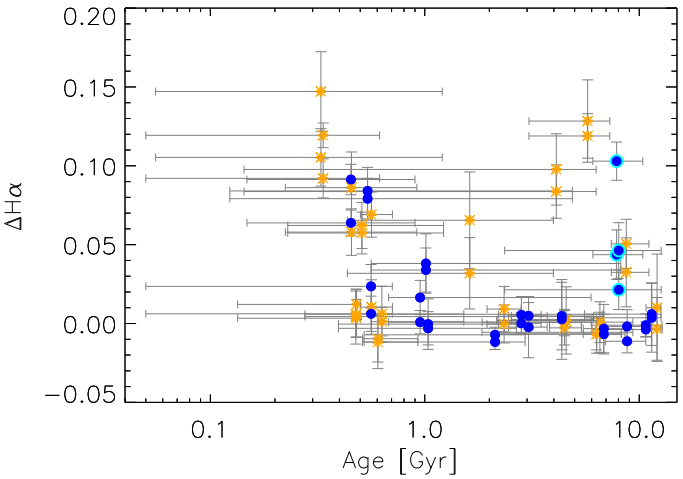

Fig. 8. Activity as a function of the age. Blue circles represent the star in Desidera et al. (2004) for which we have solid constraints on the temperature; orange crosses show the other stars. The two systems with an uncertain parallax are highlighted in cyan.

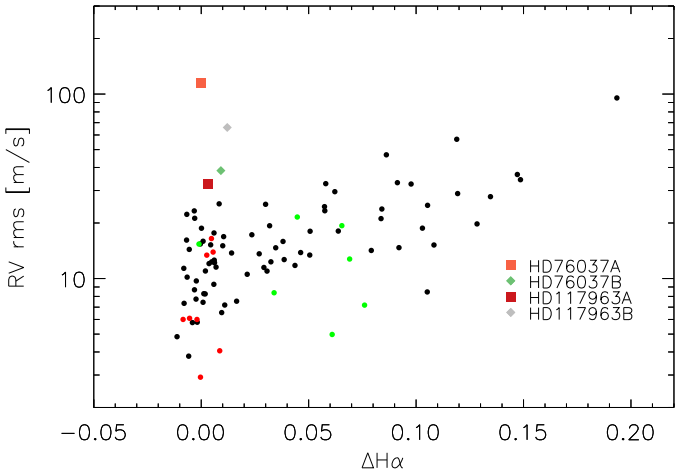

Fig. 9. Relation between the $\Delta H\alpha$ and the RV standard deviation in the survey. The green dots indicate the RV standard deviation of the stars with a known Keplerian trend that is due to a companion, in red we plot the RV standard deviation of stars with a known companion. In both cases we correct the data for their known RV variation.

are more reliable and their reference uncertainties have been estimated in ∼20 K and ∼0.06 dex, respectively. We therefore constructed a grid in $T_{\rm eff}$ and $\log g$ for each binary component, with step sizes of 25 K and 0.05 dex, respectively. We discarded all the points in the grid where the relations $\Delta T_{\rm eff} - \delta T_{{\rm eff}B} < |T_{{\rm eff}A} - T_{{\rm eff}B}| < \Delta T_{\rm eff} + \delta T_{\rm eff}$ and $\Delta \log g - \delta \log g < |\log g_A - \log g_B| < \Delta \log g + \delta \log g$ were not satisfied. We computed the ages of each component for each remaining point in the grid and retained only those for which the stars could be considered coeval ($|\log t_A - \log t_B| < 0.05$; 0.05 is the resolution of the isochrone grids). For each analysed star, we built a catalogue reporting the plausible input parameters and the resulting age that was coeval to that of its companion. For each binary system, we synthesised these data providing the youngest and oldest feasible age of the system and the median age.

In Fig. 8 we plot for each star hotter than $T_{\rm eff} = 5500$ K its $\Delta H\alpha$ as a function of the age of the system. We divided the systems into two subsamples according to the reliability of the input parameters, and in particular the $T_{\rm eff}$: blue dots represent the systems analysed in Desidera et al. (2004), which are more accurate, while orange crosses correspond to preliminary results for systems analysed in Vassallo (2014). The result shows that the majority of the active star are younger than 1.5 Gyr, while for older stars the distribution is flattened around zero, that is, they are inactive.

We found that the activity for young stars is anti-correlated with the age, confirming that the relation between the $\Delta H\alpha$ in the components of the systems younger than 1.5 Gyr is mainly due to age. The position of the pairs HD132844A and B and HD 13357A and B in the diagram of Fig. 8 does not follow the general trend: the position on colour-diagram of HD132844 below the main sequence (see Desidera et al. 2004) is indicative of substantial error in the trigonometric parallax. The two HIPPARCOS solutions for the parallax of HD13357 are inconsistent with each other. In both cases we can conclude that there is an underestimated error in the parallax. Indeed, the adopted parameters (especially the gravity) depend on the adopted trigonometric parallax: in the abundance analysis the effective temperatures were derived from ionization equilibrium and stellar gravities from luminosities, masses and temperatures, using iterative procedures. It seems therefore that a well-defined activity-age relation persists only for objects younger than ∼1.5 Gyr, and that after this age H_α seems to be less efficient as an age indicator. Our data did not show significant correlation between these quantities: due to the lack of data with such an age, we cannot conclude whether if there is a discontinuity or if the activity of the star decreases with time. The activity-age anti-correlation for younger stars confirms results from Barry (1988), for example, and the apparent flatness of the plot for older stars seems to agree with Pace (2013); but owing to the uncertainty on our ages, we cannot confirm or reject the idea that the activity decreases with age also for older stars, with a different slope as found by Mamajek & Hillenbrand (2008), for instance. Finally, we found that a large portion (15 over 35) of the stars in our sample with age estimates from the isochrone method are younger than 1.5 Gyr: this could be due to the recent bump in the star formation rate in the solar neighbourhood as claimed by Barry (1988) or to a bias in the age distribution of the stars in the HIPPARCOS Multiple Stellar Catalog. Future observations of results from the GAIA satellite may clarify this question.

5.4. Activity vs. RV scatter

We finally found the well-known relation between the activity of a star and the standard deviation of its radial velocities (Saar & Donahue 1997; Saar et al. 1998; Santos et al. 2000; Boisse et al. 2009, 2011). In addition, when considering the contamination of the spectra, we found that it is not negligible especially for the systems HD 8071, HD 99121, HD 108421 and HD 209965, which were omitted in this discussion and are detailed below. There are also a number of cases for which the spread in RV during the survey is high (>80 m/s) and which have a relatively low activity level. Most of these objects have known RV trend of Keplerian origin and after the RV variation induced by the companion was removed, they became part of the main trend (Fig. 9). In addition there are at least four stars left outside the general trend. Since these are potentially very interesting objects, we examine them more in detail.

HD 76037A and B: this is a wide binary composed of two F-type stars. The SARG spectra show that the primary star is a long-period partially blended SB2 star, therefore we conclude

Table 1. Rank of the Spearman correlation coefficient ρ_s and its significance between H_α and RV for the stars of the sample.

Star	ρ_s	σ	n_σ
HD 200466A	0.556	0.000	−4.817
HD 76037A	−0.665	0.000	3.702
HD 99121A	0.6511	0.002	−2.84
HD 213013A	0.478	0.008	−2.576
GJ 380	0.535	0.018	−2.270

Notes. Column 3 reports its false-alarm probability and the last column reports the n_σ value. Only stars with significance < 0.02 are indicated.

that the excess scatter in RVs is due to the blending of the spectra of the two components. For the secondary, the excess of the RV scatter is fairly large even after resuming the long-term trend with time that indicates the presence of a low-mass companion; in addition, the H_α index also has a trend with time – more likely related to a cycle.

The HIPPARCOS Multiple Stellar Catalog indicates that the HD 117963A system has a separation wide enough to rule out contamination effects ($\rho = 3.493''$). HD 117963B is a spectroscopic binary and some of the spectra were taken with low S/N (Desidera et al., in prep.). We cannot exclude Keplerian motion as the origin of the scatter for both stars, therefore a deeper analysis with acquisition of additional data would be required.

6. Hα index time-series analysis

By analogy with the Sun, emission in the core of H_α is expected to show time variability mainly modulated by stellar rotation over a period of the order of days, and by the activity cycle over periods of hundreds or thousands of days. In addition, secular variations in the activity levels similar to the Maunder minimum can be present. Therefore the different properties of the time series of our objects should be taken into account. Stars in the hot-Neptunes program were observed for a single season with a moderately dense sampling. In this case rotation periods could be found, but periodicities due to the activity cycle cannot be reliably identified. On the other hand, for the SARG survey objects, the observational campaign was longer and less dense. For only a few targets do we have a larger number of spectra because during the survey they were suspected to host a planet. This was the case of HD 106515A (Desidera et al. 2012) and HD 132563B (Desidera et al. 2011), for example. In addition we already know that for HD 200466A, the RV variations seen are mainly due to an activity cycle (Carolo et al. 2014).

It is known that more active stars have irregular periods that are not easy to determine with the analysis of periodograms. In spite of this, we computed the GLSPs for the H_α index that was obtained using the Zechmeister & Kürster (2009) procedure. To evaluate the significance of these periodicities, the false alarm probability (FAP) of the highest peak of the periodogram was estimated through a bootstrap method, with 1000 permutations. We used the spectral window function to rule out that our periodicity is due to the sampling. The results for the most interesting objects are listed in Table 2. We found a signature of periodic variations (rotational periods or activity cycles) in 19 stars, whereas 10 stars show a clear overall trend in H_α with time. On the other hand the stars for which we were able to find evidence of activity cycles are all with moderate activity excess and temperatures of between 4800 and 6000 K. The stars showing a long-term trend are hotter than average.

It is noteworthy that of the binary stars that show promising cycles, only HD 76037A and B are quiet and show a long-term trend.

Of the bright stars, 51 Peg was used as a RV standard to monitor instrument performances during the binary program. The quite good temporal coverage of the data allowed us to detect a significant long-term period of about seven years with FAP of 0.6%. Added to this signal, we also found a periodicity of 86.49 d, which corresponds to an alias of the 21.9 ± 0.4 d period found by Simpson et al. (2010) with one sinodic month. This shortest period seems then to be the rotational signal. We obtained a similar result also for 61 Cyg b: the GLSP peaks at 16.44 d, which is an alias of the ∼37 d period (Böhm-Vitense 2007; Oláh et al. 2009). 14 Her shows a periodicity of 22.38 d. In this case the spectral window is complex and we cannot rule out that this period is fake. Wright et al. (2004) estimated a rotational period of 48 days from the $\log R'_{HK}$ mean value, but this was not detected by Simpson et al. (2010).

All the H_α time series are available at the CDS.

7. Correlation between RV and H_α

The high uncertainty on the single measurements of H_α prevent us from properly studying the correlation with the RVs. However this was possible in some particular case, such as spectra with high S/N or stars with a relevant trend in H_α. We used the Spearman correlation coefficient ρ_S and its significance σ to quantify the correlation between RV and H_α index (Table 1): we obtained an extremely high significance for HD 200466A (see Carolo et al. 2014). For four other objects, the probability that the correlation is the result of a random effect is lower than 0.0075. HD 201936A and HD 213013A are active stars with a signature of an activity cycle, GJ 380 spectra have a high S/N and show a probable long-term cycle. Plots are presented in Appendix B. In HD 76037A the anti-correlation simply shows that both RV and activity are time-dependent on long scales. We can therefore rule out a strong physical connection between these two quantities for this star.

8. Conclusions

The activity of 104 stars observed with the SARG spectrograph was studied using an index based on the H_α line. We found that this index, $\Delta H\alpha$, correlates well with the index based on Ca II lines, $\log R'_{HK}$, and therefore it can be used to estimate the average activity level, confirming previous results. It also correlates with the rotation of the star: low activity corresponds to slow rotation, especially for cool stars. After removing a few targets for which contamination of the spectra by their companion is the dominant source of RV scatter, we found that $\Delta H\alpha$ also correlates with the scatter in RV. We obtain that a low-mass companion might be the source of a high residual RV scatter at least for HD 76073B. We also found a strong correlation between the average activity level $\langle H_\alpha \rangle$ of the two components in each binary system and that roughly a half of our systems are active. Finally, we showed that activity as measured by $\Delta H\alpha$ is correlated with the age derived from isochrone fitting. Although these have large error bars due to uncertainties in temperature and parallaxes, we found that active stars are typically younger than 1.5 Gyr, while older stars are typically inactive.

We then analysed the time series of the stars: 11 stars (∼8.5%) of the SARG sample show a periodicity in H_α with false-alarm probability <0.5%. All these stars have a moderate activity level ($0.029 < \Delta H\alpha < 0.077$) except for the pair

Table 2. Stars with cycles.

Star		$\Delta H\alpha$	Rotation [d]	Cycle [d]	Amplitude	FAP [%]
HD 186858	A	0.077	7.68	–	0.010	1.0
	B	0.062	–	2030	0.014	0.3
HD 200466	A	0.038	–	1500	0.024	<0.1
	B	0.034	–	trend	>0.015	<0.1
BD+182366	A	0.039	–	1432	0.037	0.1
	B	0.029	–	–	–	
HD 139569	A	0.057	–	trend	> 0.21	2.2
	B	0.062	–	trend	>0.30	0.6
HD 76037	A	−0.002	–	trend	>0.014	1.0
	B	0.014	–	trend	>0.022	1.3
HD 201936	A	0.059	13.70	–	0.020	0.7
	B	0.087	–	–		
HD 213013	A	0.031	–	–	–	
	B	0.035	3.59	–	0.019	2.1
14 Her		0.009	22.38	–	0.002	<0.1
51 Peg		0.003	86.49	2069	0.001, 0.003	0.8, 0.6
61 Cyg B		−0.001	16.44	–	0.011	<0.1
GJ 380		0.013	–	trend	>0.017	<0.1
τ Ceti		−0.006	–	trend	>0.003	<0.1

Notes. In the second column we indicate the component, Col. 3 reports the $\Delta H\alpha$ for the stars, Col. 4 is the short period, compatible with the rotation in our analysis (where available), Col. 5 reports the period or long-term activity cyclen Col. 6 shows the amplitude of the H_α variation. The last column indicates the false-alarm probability related to the identified periods.

HD 76037A and B, but in these cases we only have a hint of a long-term period or magnetic cycle. When we focused on the long-term cycle, we obtained that the temperature interval of these stars is also limited to late-G and early-K stars. Other stars show variabilities on temporal scales certainly different from the rotational periods. In the bright stars sample, we found five stars out of ten with significant periodic variations in H_α. In some cases the physical origin of this type of signal is unclear.

Only five stars show a significant correlation between H_α and RVs.

We conclude that if care is exerted, H_α is a useful indicator for activity and can be a good alternative to Ca II $\log R'_{HK}$ for studies based on radial velocity techniques, especially for solar-type stars.

Acknowledgements. This research has made use of the SIMBAD database, operated at CDS, Strasbourg, France. This research has made use of the Keck Observatory Archive (KOA), which is operated by the W. M. Keck Observatory and the NASA Exoplanet Science Institute (NExScI), under contract with the National Aeronautics and Space Administration. We thank the TNG staff for contributing to the observations and the TNG TAC for the generous allocation of observing time. This work was partially funded by PRIN-INAF 2008 "Environmental effects in the formation and evolution of extrasolar planetary systems".

References

Alonso, A., Arribas, S., & Martinez-Roger, C. 1996, A&A, 313, 873
Baliunas, S. L., & Vaughan, A. H. 1985, ARA&A, 23, 379
Barry, D. C. 1988, ApJ, 334, 436
Böhm-Vitense, E. 2007, ApJ, 657, 486
Boisse, I., Moutou, C., Vidal-Madjar, A., et al. 2009, A&A, 495, 959
Boisse, I., Bouchy, F., Hébrard, G., et al. 2011, A&A, 528, A4
Bonfanti, A., Ortolani, S., Piotto, G., & Nascimbeni, V. 2015, A&A, 575, A18
Bonfanti, A., Ortolani, S., & Nascimbeni, V. 2016, A&A, 585, A5
Carolo, E. 2012, Ph.D. Thesis, University of Padua, Italy
Carolo, E., Desidera, S., Gratton, R., et al. 2014, A&A, 567, A48
Charbonneau, P., & Steiner, O. 2012, Solar and Stellar Dynamos: Saas-Fee Advanced Course 39, Swiss Society for Astrophysics and Astronomy (Heidelberg, Berlin: Springer)
Cincunegui, C., Díaz, R. F., & Mauas, P. J. D. 2007, A&A, 469, 309
Desidera, S., Gratton, R. G., Scuderi, S., et al. 2004, A&A, 420, 683
Desidera, S., Gratton, R. G., Lucatello, S., & Claudi, R. U. 2006a, A&A, 454, 581
Desidera, S., Gratton, R. G., Lucatello, S., Claudi, R. U., & Dall, T. H. 2006b, A&A, 454, 553
Desidera, S., Gratton, R., Endl, M., et al. 2007, ArXiv e-prints [arXiv:0705.3141]
Desidera, S., Carolo, E., Gratton, R., et al. 2011, A&A, 533, A90
Desidera, S., Gratton, R., Carolo, E., et al. 2012, A&A, 546, A108
Dumusque, X., Lovis, C., Ségransan, D., et al. 2011, A&A, 535, A55
Endl, M., Kürster, M., & Els, S. 2000, A&A, 362, 585
Gomes da Silva, J., Santos, N. C., Bonfils, X., et al. 2011, A&A, 534, A30
Gomes da Silva, J., Santos, N. C., Boisse, I., Dumusque, X., & Lovis, C. 2014, A&A, 566, A66
Gratton, R. G., Bonanno, G., Bruno, P., et al. 2001, Exp. Astron., 12, 107
Gratton, R., Desidera, S., & Claudi, R. 2009, MSAIt, 80, 312
Gray, R. O., Corbally, C. J., Garrison, R. F., McFadden, M. T., & Robinson, P. E. 2003, AJ, 126, 2048
Isaacson, H., & Fischer, D. 2010, ApJ, 725, 875
Kürster, M., Endl, M., Rouesnel, F., et al. 2003, A&A, 403, 1077
Kurucz, R. L., Furenlid, I., Brault, J., & Testerman, L. 1984, Solar flux atlas from 296 to 1300 nm
Lovis, C., Dumusque, X., Santos, N. C., et al. 2011, ArXiv e-prints [arXiv:1107.5325]
Mamajek, E. E., & Hillenbrand, L. A. 2008, ApJ, 687, 1264
Martínez Fiorenzano, A. F., Gratton, R. G., Desidera, S., Cosentino, R., & Endl, M. 2005, A&A, 442, 775
Meunier, N., & Delfosse, X. 2009, A&A, 501, 1103
Noyes, R. W., Hartmann, L. W., Baliunas, S. L., Duncan, D. K., & Vaughan, A. H. 1984, ApJ, 279, 763
Oláh, K., Kolláth, Z., Granzer, T., et al. 2009, A&A, 501, 703
Pace, G. 2013, A&A, 551, L8
Pace, G., Melendez, J., Pasquini, L., et al. 2009, A&A, 499, L9

Perryman, M. A. C., Lindegren, L., Kovalevsky, J., et al. 1997, A&A, 323, L49
Queloz, D., Henry, G. W., Sivan, J. P., et al. 2001, A&A, 379, 279
Robertson, P., Mahadevan, S., Endl, M., & Roy, A. 2014, Science, 345, 440
Robinson, R. D., Cram, L. E., & Giampapa, M. S. 1990, ApJS, 74, 891
Saar, S. H., & Donahue, R. A. 1997, ApJ, 485, 319
Saar, S. H., Butler, R. P., & Marcy, G. W. 1998, ApJ, 498, L153
Santos, N. C., Mayor, M., Naef, D., et al. 2000, A&A, 361, 265
Santos, N. C., Gomes da Silva, J., Lovis, C., & Melo, C. 2010, A&A, 511, A54
Simpson, E. K., Baliunas, S. L., Henry, G. W., & Watson, C. A. 2010, MNRAS, 408, 1666
Skumanich, A. 1972, ApJ, 171, 565
Soderblom, D. R., Stauffer, J. R., Hudon, J. D., & Jones, B. F. 1993, ApJS, 85, 315
Strassmeier, K. G., Fekel, F. C., Bopp, B. W., Dempsey, R. C., & Henry, G. W. 1990, ApJS, 72, 191
Strassmeier, K., Washuettl, A., Granzer, T., Scheck, M., & Weber, M. 2000, A&AS, 142, 275
Tody, D. 1993, in Astronomical Data Analysis Software and Systems II, eds. R. J. Hanisch, R. J. V. Brissenden, & J. Barnes, ASP Conf. Ser., 52, 173
Valenti, J. A., & Fischer, D. A. 2005, ApJS, 159, 141
Vassallo, D. 2014, Master's Thesis, Universita' degli Studi di Bologna, Italy
Vaughan, A. H., & Preston, G. W. 1980, PASP, 92, 385
Voges, W., Aschenbach, B., Boller, T., et al. 1999, A&A, 349, 389
Voges, W., Aschenbach, B., Boller, T., et al. 2000, IAU Circ., 7432, 1
Wright, J. T., Marcy, G. W., Butler, R. P., & Vogt, S. S. 2004, ApJS, 152, 261
Zechmeister, M., & Kürster, M. 2009, A&A, 496, 577
Zhao, J. K., Oswalt, T. D., Rudkin, M., Zhao, G., & Chen, Y. Q. 2011, AJ, 141, 107

Appendix A: Additional tables

Table A.1. Stellar parameters.

Star	V	$B-V$	$\log R'_{HK}$	Method	$v \sin i$ [km s^{-1}]	T_{eff} [K]
BD 182366A	9.370	0.83	−4.56	U	2.0	5308
BD 182366B	9.427	0.93	−4.57	U	2.4	5290
BD 222706A	9.594	0.62	−4.97	D	2.3	5943
BD 222706B	9.828	0.69	−4.51	U	2.3	5674
BD 231978A	9.395	0.83	−4.46	D	3.5	4886
BD 231978B	9.530	0.75	−4.44	U	3.2	4911
HD 105421A	7.827	0.51	−4.70	U	4.6	6324
HD 105421B	8.358	0.57	−4.65	U	0.9	6102
HD 106515A	7.960	0.79	−5.04	D	1.7	5314
HD 106515B	8.234	0.83	−5.07	D	1.8	5157
HD 108421A	8.870	0.90	−4.57	X	2.6	4700
HD 108421B	9.274	0.88	−4.53	X	3.2	4779
HD 108574	7.418	0.56	−4.49	D	4.9	6205
HD 108575	7.972	0.67	−4.43	X	5.1	5895
HD 109628A	9.073	0.57	−4.51	U	3.0	6109
HD 109628B	9.087	0.55	−4.50	U	3.2	6127
HD 117963A	8.639	0.55	−4.65	U	6.2	6180
HD 117963B	8.924	0.49	−4.61	U	3.3	6097
HD 118328A	9.147	0.62	−4.61	U	0.7	5943
HD 118328B	9.426	0.69	−4.59	U	0.7	5887
HD 121298A	8.604	0.50	−4.91	D	1.9	6353
HD 121298B	8.937	0.52	−4.87	D	1.3	6266
HD 123963A	8.758	0.62	−4.63	U	1.6	5873
HD 123963B	9.511	0.60	−4.55	U	1.4	5438
HD 124054A	8.399	0.58	−4.97	D	2.7	6081
HD 124054B	8.785	0.64	−5.02	D	2.5	5896
HD 126246A	7.466	0.54	−4.40	D	7.9	6223
HD 126246B	7.697	0.60	−4.51	D	3.9	6074
HD 128041A	8.059	0.71	−4.53	U	3.4	5663
HD 128041B	8.827	0.78	−4.51	U	3.2	5192
HD 132563A	8.948	0.54	−4.62	U	3.9	6168
HD 132563B	9.402	0.57	−4.62	U	3.4	5985
HD 132844A	9.022	0.55	−4.66	U	3.4	5878
HD 132844B	9.114	0.63	−4.61	U	2.4	5809
HD 13357A	8.180	0.67	−4.70	D	1.7	5615
HD 13357B	8.647	0.73	−4.61	D	1.8	5341
HD 135101A	6.656	0.69	−4.99	D	2.3	5631
HD 135101B	7.500	0.75	−5.07	D	1.1	5491
HD 139569A	8.482	0.54	−4.55	U	8.5	6223
HD 139569B	8.783	0.57	−4.52	U	5.6	5922
HD 143144A	8.856	0.62	−4.61	U	1.9	5943
HD 143144B	9.025	0.61	−4.59	U	1.2	5894
HD 146413A	9.260	0.88	−4.68	D	2.1	4779
HD 146413B	9.492	0.87	−4.60	X	2.0	4818
HD 17159A	8.775	0.54	−4.64	U	3.4	6155
HD 17159B	8.923	0.53	−4.62	U	2.9	6051
HD 186858A	8.368	0.96	−4.73	D	3.6	4910
HD 186858B	8.578	0.93	−4.62	X	3.0	4885
HD 190042A	8.755	0.73	−4.71	U	3.5	5474
HD 190042B	8.778	0.80	−4.72	U	3.8	5406
HD 19440A	7.874	0.47	−4.73	U	4.5	6308
HD 19440B	8.574	0.53	−4.66	U	2.9	6108
HD 200466A	8.399	0.74	−4.77	D	2.0	5633

Notes. For each star we indicate the apparent V magnitude, the $B-V$ color index, the method used to calculate $\log R'_{HK}$ and its value, the projected velocity $v \sin i$ and temperature. $\log R'_{HK}$ values were derived from direct measurement (D) of other authors, from the X-ray luminosity (X), or can be only an upper limits (U), still from X-ray luminosity data.

Table A.1. continued.

Star	V	$B-V$	$\log R'_{HK}$	Method	$v \sin i$ [km s^{-1}]	T_{eff} [K]
HD 200466B	8.528	0.76	−4.69	D	2.1	5583
HD 201936A	8.648	0.48	−4.55	X	8.8	6441
HD 201936B	8.851	0.50	−4.53	X	15.5	6452
HD 209965A	7.980	0.55	−4.96	D	4.2	6180
HD 209965B	8.414	0.57	−4.59	U	2.1	6115
HD 213013A	8.982	0.81	−4.59	U	1.7	5402
HD 213013B	9.612	0.93	−4.53	U	2.3	4990
HD 215812A	7.275	0.64	−4.66	U	1.3	5688
HD 215812B	7.576	0.71	−4.64	U	1.5	5586
HD 216122A	8.062	0.58	−4.73	U	6.5	6067
HD 216122B	8.186	0.58	−4.71	U	4.6	6066
HD 219542A	8.174	0.64	−5.07	D	2.1	5849
HD 219542B	8.547	0.72	−4.81	D	1.9	5691
HD 2770A	9.566	0.61	−4.39	X	2.8	5970
HD 2770B	9.660	0.73	−4.39	X	3.9	5844
HD 30101A	8.782	0.82	−4.72	D	1.9	5143
HD 30101B	8.848	0.91	−4.79	D	2.2	5061
HD 33334A	8.023	0.70	−4.99	D	1.9	5650
HD 33334B	8.857	0.80	−4.63	U	1.7	5201
HD 66491A	9.253	0.75	−4.65	D	2.5	5497
HD 66491B	9.312	0.67	−4.58	D	2.4	5492
HD 76037A	7.688	0.50	−5.14	D	7.9	6353
HD 76037B	8.269	0.50	−5.03	D	9.5	6442
HD 8009A	8.819	0.64	−4.96	D	0.2	5688
HD 8009B	9.724	0.82	−4.95	D	0.0	5291
HD 8071A	7.312	0.57	−4.74	U	5.5	6218
HD 8071B	7.573	0.60	−4.71	U	6.0	6142
HD 85441A	8.907	0.70	−4.60	X	1.3	5701
HD 85441B	9.284	0.71	−4.56	X	1.6	5537
HD 86057A	8.839	0.60	−4.49	X	6.0	6012
HD 86057B	9.676	0.73	−4.40	X	4.6	5629
HD 87743A	8.734	0.62	−4.71	D	2.5	5943
HD 87743B	8.890	0.60	−4.59	D	3.0	5905
HD 94399A	9.407	0.61	−4.54	X	3.2	5970
HD 94399B	9.306	0.71	−4.56	X	3.6	6017
HD 9911A	9.428	0.90	−4.60	U	1.3	5000
HD 9911B	9.448	0.89	−4.60	U	1.3	4968
HD 99121A	8.162	0.46	−4.67	U	6.7	6501
HD 99121B	9.018	0.47	−4.57	U	5.0	6374
HIP 104687A	8.144	0.64	−4.41	D	3.0	5870
HIP 104687B	8.189	0.71	−4.48	D	3.4	5801
14 Her	6.610	0.88	−5.06	D	1.6	5388
40 Eri	4.430	0.65	−4.90	D	0.5	5151
51 Peg	5.450	0.67	−5.08	D	2.0	5787
61 Cyg B	6.030	1.31	−4.95	D	1.7	4077
83 LeoA	6.490	1.00	−4.84	D	1.4	5502
GJ 380	6.610	1.33	−4.72	D	1.9	3876
GJ 580A	6.580	0.78	−5.11	D	2.1	5174
HD 166435	6.840	0.58	−4.27	D	7.6	5964
ρ CrB	5.390	0.61	−5.08	D	1.0	5823
τ Cet	3.490	0.73	−4.98	D	1.0	5283

Table A.2. SARG data.

Star	No. obs	JD_0	JD_F	$\langle H\alpha \rangle$	$\Delta H\alpha$	$\sigma_{H\alpha}$	RV [km s^{-1}]	rms(RV) [m/s]
BD+182366A	20	1985.4166	4251.3874	0.255	0.039	0.025	11.00	12.67
BD+182366B	18	1985.4317	4251.3989	0.246	0.029	0.021	11.40	11.48
BD+222706A	18	2011.6073	4309.4345	0.225	0.008	0.019	−4.10	25.41
BD+222706B	18	2011.6264	4962.4638	0.258	0.045	0.012	2.41	21.55
BD+231978A	14	1825.7278	4398.6806	0.371	0.135	0.027	20.50	28.41
BD+231978B	13	1825.7152	4398.6929	0.383	0.149	0.025	23.50	35.19
HD 105421A	21	2011.4704	4902.4194	0.237	0.010	0.017	7.40	16.87
HD 105421B	19	2011.4840	4902.4333	0.290	0.069	0.014	0.44	12.76
HD 106515A	31	1986.5327	6026.5634	0.214	−0.002	0.006	0.43	6.00
HD 106515B	30	1986.5442	6026.5757	0.218	−0.003	0.007	18.80	8.69
HD 108421A	17	1986.5975	4250.4681	0.296	0.044	0.007	2.00	21.82
HD 108421B	13	2012.4862	4250.4796	0.360	0.116	0.018	2.00	38.30
HD 108574	22	1913.7615	4251.4385	0.287	0.064	0.008	−2.10	18.09
HD 108575	22	1913.7846	4251.4499	0.307	0.091	0.010	−1.50	33.09
HD 109628A	14	1986.5683	4961.3994	0.214	−0.007	0.012	0.00	10.18
HD 109628B	13	1986.5799	4961.4117	0.215	−0.007	0.010	0.00	16.16
HD 117963A	15	2012.5413	5968.6519	0.226	0.003	0.012	−5.80	33.22
HD 117963B	13	2012.5543	5968.6641	0.233	0.012	0.010	4.18	66.04
HD 118328A	15	2013.6231	4252.5454	0.212	−0.006	0.013	19.20	14.38
HD 118328B	14	2013.6353	4250.5043	0.217	0.001	0.013	18.40	15.93
HD 121298A	14	1912.7867	4161.5587	0.229	0.001	0.009	0.00	8.28
HD 121298B	12	1912.7733	4161.5702	0.231	0.006	0.018	0.00	12.58
HD 123963A	15	2011.5410	4309.4080	0.222	0.006	0.011	−24.40	12.23
HD 123963B	13	2011.5537	4309.4202	0.238	0.024	0.014	−24.40	17.28
HD 124054A	13	2011.5702	4251.4849	0.222	0.002	0.004	−14.60	8.25
HD 124054B	14	2011.5833	4251.4964	0.218	0.002	0.021	−13.40	10.99
HD 126246A	18	2012.5729	4488.7666	0.343	0.119	0.008	0.80	28.88
HD 126246B	16	2012.5846	4311.3850	0.312	0.092	0.012	1.70	14.71
HD 128041A	23	2013.4984	4276.4738	0.210	−0.003	0.020	−74.70	7.45
HD 128041B	21	2013.5115	4276.4852	0.230	0.010	0.034	−73.60	16.31
HD 132563A	63	2013.6508	5968.6857	0.227	0.005	0.021	1.80	16.47
HD 132563B	56	2013.6645	5968.7008	0.221	0.003	0.025	1.65	13.39
HD 132844A	27	2012.6152	4311.4244	0.259	0.044	0.016	−3.20	11.87
HD 132844B	26	2012.6027	4311.4359	0.318	0.103	0.012	−2.00	18.84
HD 13357A	29	1801.6950	4849.4490	0.235	0.021	0.013	26.20	10.55
HD 13357B	25	1801.7086	4849.4612	0.262	0.046	0.018	25.40	13.83
HD 135101A	14	1982.7540	4488.7807	0.202	−0.011	0.007	0.00	4.84
HD 135101B	12	1982.7697	4311.4614	0.212	−0.002	0.011	0.00	5.80
HD 139569A	18	2012.6615	4339.4064	0.281	0.057	0.013	−29.40	24.53
HD 139569B	20	2012.6733	4339.4179	0.279	0.062	0.015	−29.80	29.57
HD 143144A	19	1798.3625	4339.3805	0.223	0.006	0.015	−78.50	9.39
HD 143144B	18	1798.3768	4339.3923	0.221	0.004	0.017	−78.80	15.29
HD 146413A	20	2012.6910	4962.5618	0.350	0.105	0.013	4.20	8.61
HD 146413B	19	2012.7035	4962.5734	0.350	0.108	0.020	5.30	15.32
HD 17159A	28	1797.6565	4819.3558	0.219	−0.003	0.011	11.40	21.43
HD 17159B	28	1797.6727	4819.3679	0.219	−0.000	0.016	10.20	15.88
HD 186858A	44	1798.4744	4962.5879	0.310	0.076	0.010	−0.63	8.90
HD 186858B	41	1798.4601	4962.6015	0.297	0.061	0.013	1.54	7.64
HD 190042A	23	1825.4814	4783.3459	0.210	−0.004	0.010	−4.60	5.77
HD 190042B	22	1825.4615	4783.3593	0.212	−0.002	0.012	−3.50	7.74
HD 19440A	19	1828.6588	4339.6564	0.231	0.005	0.008	−15.40	12.31
HD 19440B	19	1828.6716	4339.6679	0.219	−0.002	0.019	−15.90	9.70
HD 200466A	79	1801.5721	5807.6025	0.251	0.038	0.019	−8.00	15.89
HD 200466B	71	1801.5850	5807.6137	0.247	0.034	0.014	−0.22	8.37
HD 201936A	15	2042.6381	4398.3978	0.289	0.058	0.015	3.70	32.87
HD 201936B	15	2042.6554	4398.4092	0.317	0.086	0.023	2.50	47.51

Notes. For each star we indicate the number of observations acquired during the SARG survey, the data (JD-2 450 000) of the first and the last point, the average value of H_α, the value of $\Delta H\alpha$ and of the standard deviation of the points. In the last two columns we indicate the mean value of the RVs and its standard deviation, corrected for the known Keplerian motion, if applicable.

Table A.2. continued.

Star	No. obs	JD_0	JD_F	$\langle H\alpha \rangle$	$\Delta H\alpha$	$\sigma_{H\alpha}$	RV [km s^{-1}]	rms(RV) [m/s]
HD 209965A	26	2145.5472	4783.3759	0.223	0.001	0.008	−19.40	20.60
HD 209965B	22	2145.5634	4783.3878	0.218	−0.003	0.011	0.11	24.31
HD 213013A	34	1827.4669	4369.5700	0.245	0.031	0.016	−24.70	10.98
HD 213013B	32	1827.4540	4369.5824	0.264	0.035	0.024	−24.70	14.68
HD 215812A	29	1798.4923	4398.4798	0.210	−0.004	0.005	8.43	32.68
HD 215812B	18	1798.5063	4398.4912	0.212	−0.001	0.007	0.95	20.25
HD 216122A	24	1801.6229	4962.6771	0.220	0.000	0.007	−13.30	18.74
HD 216122B	27	1801.6366	4962.6895	0.225	0.006	0.012	−1.04	13.92
HD 219542A	43	1825.5176	4664.6807	0.216	0.001	0.007	−12.50	7.43
HD 219542B	48	1825.5048	4664.6931	0.230	0.016	0.011	−11.50	7.54
HD 2770A	21	1856.5704	4338.6438	0.301	0.084	0.017	−5.00	21.13
HD 2770B	21	1856.5841	4338.6587	0.313	0.098	0.023	−6.40	32.54
HD 30101A	33	1825.6514	5952.4781	0.252	0.030	0.021	−18.20	25.26
HD 30101B	33	1825.6652	5952.4943	0.252	0.027	0.023	−18.00	13.62
HD 33334A	57	1801.7517	5952.5179	0.207	−0.007	0.013	83.20	22.28
HD 33334B	51	1801.7439	5952.5299	0.216	−0.003	0.015	83.70	23.26
HD 66491A	24	1853.7409	4398.7585	0.264	0.051	0.023	48.40	18.04
HD 66491B	21	1853.7557	4161.4142	0.271	0.058	0.030	49.10	23.30
HD 76037A	35	1828.7406	5952.6152	0.228	−0.000	0.012	22.02	114.52
HD 76037B	34	1853.7833	5952.6280	0.240	0.009	0.014	−0.05	38.46
HD 8009A	33	2116.6201	4819.3811	0.217	0.004	0.022	−42.10	12.05
HD 8009B	26	2116.6334	4819.3929	0.223	0.006	0.020	−41.80	17.66
HD 8071A	12	1797.6224	4339.6225	0.217	−0.007	0.005	5.67	18.94
HD 8071B	9	1797.6397	3246.6791	0.210	−0.012	0.005	9.00	64.80
HD 85441A	15	1826.7408	4754.7425	0.246	0.032	0.022	−19.80	12.32
HD 85441B	15	1826.7535	4754.7538	0.264	0.051	0.016	−19.80	13.42
HD 86057A	18	1985.5083	4251.3612	0.324	0.105	0.018	11.80	24.94
HD 86057B	18	1985.5216	4251.3726	0.360	0.147	0.025	11.20	36.64
HD 87743A	23	2012.3936	4849.6255	0.249	0.032	0.023	0.00	19.33
HD 87743B	25	2012.3801	4849.6371	0.282	0.065	0.031	3.00	19.35
HD 94399A	19	1986.4614	4962.3837	0.346	0.128	0.026	−6.20	20.16
HD 94399B	17	1986.4731	4962.3953	0.338	0.119	0.014	−3.80	57.20
HD 9911A	22	1801.6656	4339.6330	0.236	0.007	0.030	−56.60	11.53
HD 9911B	20	1801.6528	4339.6445	0.223	−0.008	0.021	−56.30	11.36
HD 99121A	24	1986.5086	4250.4427	0.223	−0.010	0.015	−4.40	23.66
HD 99121B	20	1986.5205	4250.4552	0.217	−0.012	0.017	−3.10	30.57
HIP 104687A	30	2070.6622	4309.6015	0.300	0.084	0.015	−20.60	23.82
HIP 104687B	29	2070.6751	4309.6148	0.294	0.079	0.013	−21.20	14.20
14 Her	144	4515.7409	4902.6461	0.223	0.009	0.003	−2.97	4.06
40 Eri	42	4515.3574	4819.4971	0.232	0.011	0.002	−42.20	7.19
51 Peg	44	1774.6139	4783.4387	0.206	−0.009	0.003	0.57	6.00
61 Cyg B	127	2570.3207	4693.6690	0.343	−0.001	0.008	−0.29	2.92
83 Leo A	121	4512.5548	4819.6320	0.223	0.009	0.003	−2.90	6.54
GJ 380	145	4512.4711	4819.5728	0.403	0.013	0.012	−26.10	5.39
GJ 580 A	158	4512.6957	4694.3972	0.213	−0.008	0.004	−67.90	7.34
HD 166435	18	2775.6448	3872.7162	0.411	0.193	0.010	−13.70	95.27
ρ CrB	46	2011.7355	4663.5609	0.210	−0.006	0.004	−1.32	6.09
τ Cet	225	1773.7347	4819.3086	0.211	−0.006	0.003	−16.40	4.86

Appendix B: Stars with RV-H_α correlation

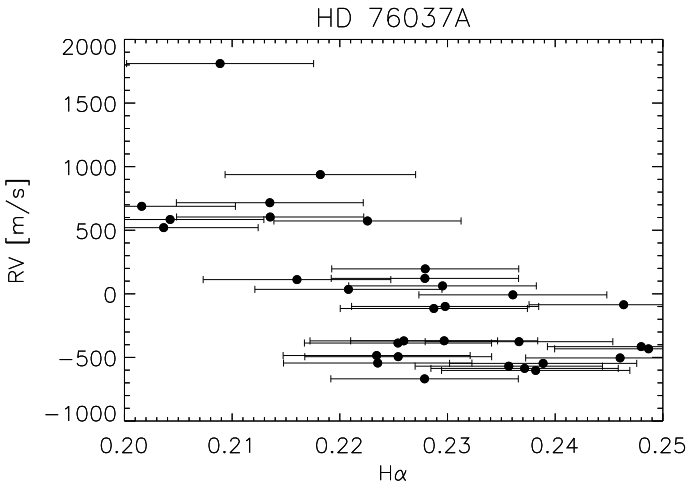

Fig. B.1. RV as a function of the H_α index for HD 76037A.

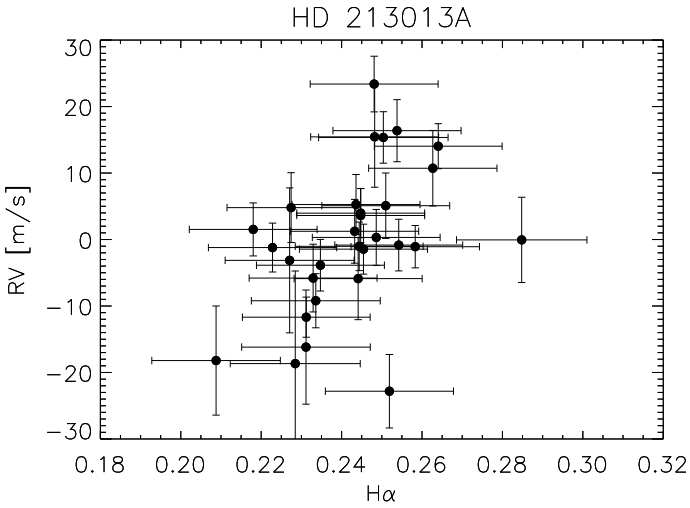

Fig. B.2. RV as a function of the H_α index for HD 213013A.

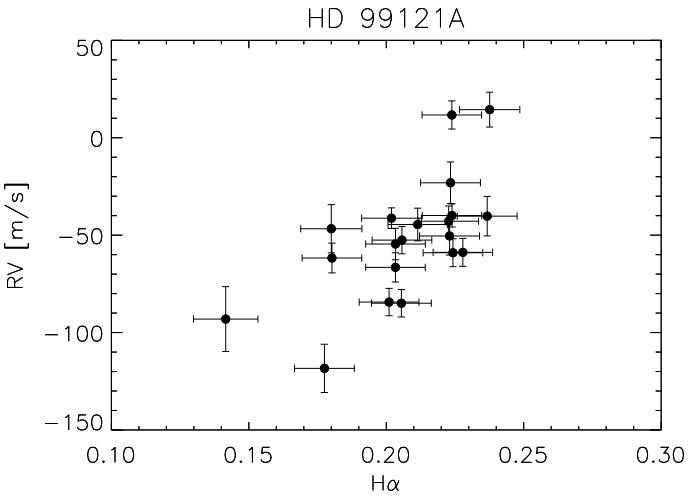

Fig. B.3. Decontaminated RV as a function of the H_α index for HD 99121A.

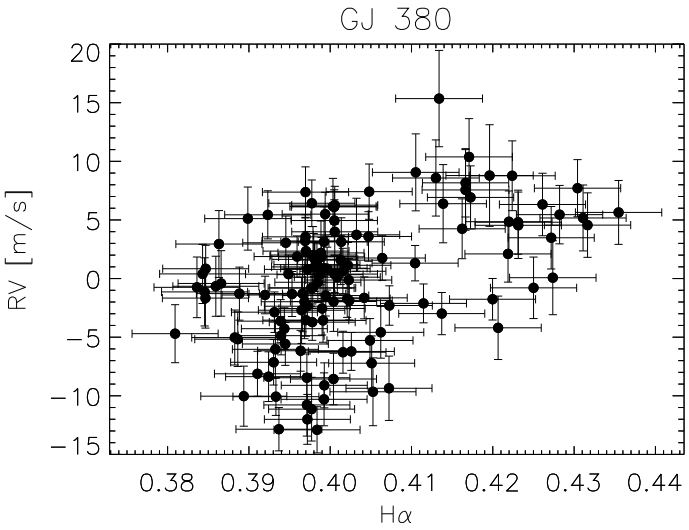

Fig. B.4. RV as a function of the H_α index for GJ 380.